Int J Thermophys (2016) 37:67
DOI 10.1007/s10765-016-2072-y

ICPPP 18

Thermal Lens Spectrometry: Still a Technique on the Horizon?

Mingqiang Liu[1,2] · **Mladen Franko**[1]

Received: 14 October 2015 / Accepted: 28 April 2016 / Published online: 12 May 2016

Abstract In this article, the historical development of thermal lens spectrometry (TLS) is briefly reviewed as an introduction. In continuation, the emphasis is on the recent progresses of TLS for measurements in ensembled sample cells and in microfluidic flow injection systems. Novel theories, instrumentation and their applications for high sample throughput for environmental, chemical and biomedical analysis, as well as thermal characterization and imaging, particularly in microspace, are presented. Discussion is given on the limitations of present TLS systems that open new horizons for future progress of this technique, which has already found place among routine techniques for chemical analysis. In the final section, proposals for the future development of TLS towards advanced applications in new research fields are presented.

Keywords Biomedical assay · Chemical analysis · Environmental monitoring · Microfluidic chip · Thermal lens spectrometry

This article is part of the selected papers presented at the 18th International Conference on Photoacoustic and Photothermal Phenomena.

✉ Mingqiang Liu
mqliu@swust.edu.cn

✉ Mladen Franko
mladen.franko@ung.si

1 Laboratory for Environmental Research, University of Nova Gorica, Vipavska 13, P.O. Box 301, 5000 Nova Gorica, Slovenia

2 School of Science, Southwest University of Science and Technology, Mianyang 621010, China

1 Introduction

Since its emergence in 1965, thermal lens spectrometry (TLS) [1] has been extensively investigated and subsequently applied for thermophysical or chemical characterization [2,3] of various materials. TLS relies on probing a refractive index change induced by nonradiative relaxation of the energy absorbed in a sample irradiated by a laser beam. As such, TLS was mainly used for detecting nonfluorescent analytes, although it was also applied to fluorescent compounds with fluorescence quantum yield smaller than one.

From the 1960s to 1980s, TLS was developed from the initial single-beam scheme to a dual-beam configuration [4], which enhanced the system's flexibility and detection sensitivity. In the 1980s, different TLS theoretical models (under parabolic approximation or considering the aberrant nature of thermal lens) were developed for static or flowing samples, excited by a modulated continuous-wave (CW) laser or by a pulsed laser [5]. Through these theoretical achievements and experimental optimization, TLS has reached ultra-high sensitivity (capable of detecting an absorbance of 10^{-7} AU or less), low detection volume (sub μL) capability, and was regarded as one of the promising spectrochemical techniques on the horizon [6]. However, TLS instruments at that time were still bulky and their selectivity was poor due to limited available laser emission lines.

Between the 1990s and early 2000s, on one hand, researchers were trying to improve the TLS [5,7,8] for (i) better sensitivity by optimizing experimental systems through more rigorous theoretical modelling (such as mode-mismatched dual-beam TLS for cw laser excitation), (ii) detecting a wider range of analytes in a larger variety of samples through new TLS schemes (e.g. differential TLS for sample with high background absorbance, phase-conjugate TLS for optically inhomogeneous samples, and circular dichroism-TLS for optically active samples), (iii) multiwavelength or broadband detection by using multiline/broadband light sources or by extending into infrared/ultraviolet spectral regions, (iv) improved selectivity by coupling to separation techniques (liquid chromatography, capillary electrophoresis, etc.) or bioanalytical methods (enzymatic reactions or immunoassays). On the other hand, miniaturized TLS instrumentation, namely a thermal lens microscope (TLM), such as developed by Kitamori et al. [9] for chemical analysis in microspace, especially when microfluidic chips opened new research opportunities. TLM offered a very low mass detection limit (down to 0.4 molecules in a detection volume of a few fL). Advantages of TLM over TLS, such as high spatial and temporal resolutions as well as compactness and portability, enabled TLM to become a very promising optical probing technique in lab-on-a-chip technologies. However, its concentration detection sensitivity was still not as high as in conventional TLS due to its limitation of over 100 times shorter an optical pathlength in a microchip in comparison with a 1 cm sample cuvette as it is usually the case for TLS.

Over the past decade, TLS refined theoretical methods (by including the Soret effect [10,11], molecular heat convection [12] and photochemical reactions [13,14], or effects as in the case of nanoparticle ensembles [15]) and in optical schemes (such as collimated probe beam TLS [16,17]), which has resulted in various applications. These include studying processes such as phase transitions [18,19] (or conversely,

over 10-fold enhancement of the photothermal signal by exploitation of the thermotropic phase transitions [20,21]) or characterization of different materials (biodiesels [22,23], metallic colloids [24,25], nanocomposites (carbon nanomaterials) [26–28] and chemical or biological compounds [29,30]) or by imaging of chromophores in biological cells [31]. On the other hand, rapid developments in theories and instruments were also observed for TLM, which found extensive applications for chemical and biological/biomedical analysis by coupling with microscale analytical devices (especially microfluidic chips). In theory, different models considering impacts of the sample's surroundings on the TLM signal [32], or employing a confocal scheme for higher spatial resolution [33], or based on the exact generalized Lorenz-Mie theory (GLMT) for detection of a single nanoparticle (NP) [34] were developed. Correspondingly, TLM instruments with adjustable beam parameters [35,36], integrated on a microchip [37], with optical near-field detection for nonabsorbing molecules [38] or with highly focused pump-probe beams [34] were developed. Other instrumental schemes (circular dichroism TLM [39], polarization modulation TLM [40], differential interference contrast TLM [41]), were designed for chemical analysis when coupled to a micro-HPLC [42]. For high sample throughput analysis of environmental [43] and biological/clinical samples [44], TLM was combined with microfluidic flow injection analysis. Biological (cellular) imaging [45,46], in-chip investigations of multiphase molecular diffusion [47], detection of trace amounts of analytes in extended nanofluidic channels [48], or characterization of single molecule or nanoparticles [49,50] were also reported.

With these achievements, it appears that TLS and TLM have reached substantial level of maturity, which make them ready for routine chemical analysis, as have been outlined in several recent articles [8,51–54]. There are, however, still many research areas deserving our attention in order to advance TLS/TLM for chemical analysis and many new applications. In this paper, we will give an overview of the quite recent developments in TLS/TLM, which are not discussed or only briefly mentioned in already published review articles.

2 Development of TLS Theoretical Models and Instruments

In this section, we first introduce the progress in theoretical models and instruments used for analysis of an ensemble of analyte, in which the TL signal can be described by Fresnel diffraction theory only if the analyte molecule is much smaller than the probe beam size in the sample. Then, those developments for single nanoparticle detection will be described, where usually GLMT was used for photothermal signal analysis.

2.1 TLS for Detection in an Ensembled Sample or Sample Cell

When TLS is applied for detection in microspace, the sample surroundings or sample's physical state could have a significant influence on the TLS detection. In our recent research, we have theoretically and experimentally analysed the impacts of the surroundings [32,35,36], as well as the flow of the sample [55,56]. It is obviously necessary to consider the impact of the surroundings if this would alter the TL

effect on the sample itself. Such interference could be positive or negative, which means amplifying or decreasing the TL effect. Therefore, by investigating the impacts at given experimental conditions, we could have a better understanding of the heat generation, diffusion and TL effect in microspace, based on which, new ways for enhancing the TL signal and consequently the detection sensitivity could be found. For example, we studied the case of detecting an aqueous sample in a conventional microfluidic chip with 100 μm deep and 200 μm wide channel, and we conclude that the following:

(1) Qualitatively speaking, when the thermal diffusion length around the signal generation volume is smaller than the dimension of the sample compartment, the impact of the surroundings can be neglected, otherwise they should be considered. When a laser is used for excitation, high focusing of the objective lens (OL) keeps the laser spot in the sample quite small (∼1 μm or less), and the thermal diffusion length $D_{th} = (D/\pi f)^{1/2}$ is 6.7 μm at $f = 1$ kHz . For the microchannel mentioned above, impacts from the channel walls on the TL signal can be neglected. However, when an incoherent light source is employed as the excitation beam, the channel wall has a significant effect on the TL signal amplitude, since the ILS beam can hardly be focused to a very small point if we want to keep a relatively high excitation power. For example, for an ILS beam with a beam size of 230 μm (and a "Rayleigh range" of 450 μm, which was defined similar to that of a laser beam [32]) in the sample, and a thermal diffusion length of 48 μm at $f = 20$ Hz, the heat diffuses into the surrounding layers and behaves as an additional positive or negative thermal lens element, depending on whether the sign of the thermo-optical parameter (dn/dT) of the surroundings is the same or opposite to that of the sample (Fig. 1a). The TL signal for an octane/sample/octane ensembled system is about seven times higher than that of a fused silica/sample/fused silica system, as shown in Fig. 1b. Further decreasing the modulation frequency will enlarge the difference. In experimentation, we obtained a signal enhancement of about nine-fold at $f = 5$ Hz by using octane as the surrounding layers. However, in practical applications, especially in a closed microchannel, it is difficult to use organic solvents as an additional signal enhancement layer, and instead, a material with good thermo-optical properties (high dn/dT and low k), good physical and chemical stability and easiness of deposition on channel walls should be chosen as the additional layer.

(2) When the sample flows, the TL element can be distorted depending on whether the flow distance in one excitation cycle is of similar dimension to the TL element or larger. For example, at $f = 1$ kHz for a laser excitation, the flow velocity is 30 mm/s when the flow distance is equal to the size of the TL element (here, defined as $2D_{\text{th}}$). As shown in Fig. 1c, at $v_x = 30$ mm/s , the signal decrease, induced by the sample flow, is quite apparent. The difference between the theoretical and experimental values comes from the theoretical assumption of homogeneous flow of the liquid in the channel, which is half of the maximum flow velocity for a real (laminar) flow. By offsetting the pump and probe beams in the flow direction to compensate for the flow-induced TL element distortion, the signal decrease can be avoided to some extent, and the response linearity of the system is also improved [55].

(3) When the pump beam is highly focused (usually the case in TLM) and the sample length along the optical axis is much larger than the Rayleigh range of the

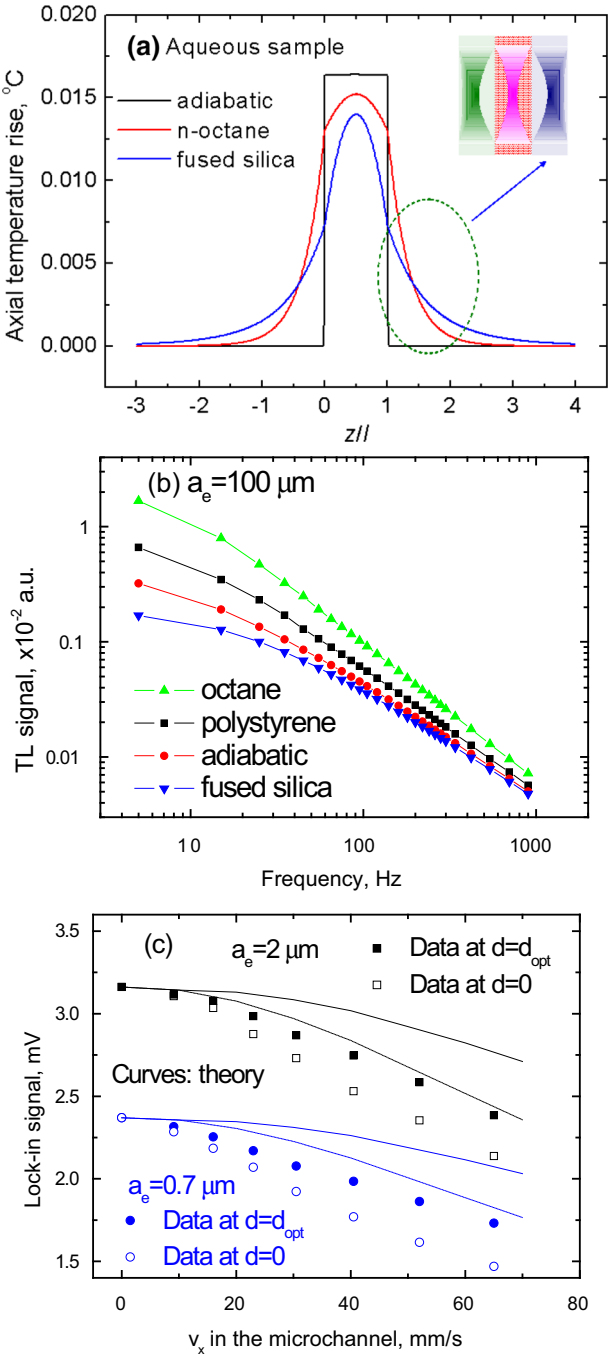

Fig. 1 (a) Axial (z-direction) temperature distribution in three-layer systems. Both l and a_e are 100 µm and the modulation frequency is 20 Hz. (b) Frequency-dependent TL signals. (c) TL signal as a function of flow velocity in the microchannel for two-pump beam profiles at two beam offsets (d)

laser, the effect of beam divergence in the pump beam on the TL element formation and probe beam detection should be considered [35]. At $f = 1$ kHz , the effective TL element thickness was found to be $6z_{ce}$ (with z_{ce} the confocal distance of the excitation beam). This thickness is usually much larger than the confocal distance of the probe beam (about 5 μm for $w_1 = 1\,\mu m$), which necessitates considering a "finite TL element" for the optimization of on-axis relative distance of the probe and pump waists for the highest sensitivity. In addition, we found that for a relatively large sample length (e.g. >100 μm), the optimum pump beam waist radius was $[\lambda_e l/(4\pi)]^{1/2}$. At optimum pump beam waist, the sensitivity achieves maximum at a much lower power density (1/10) than that for the diffraction-limited excitation in the sample.

(4) To achieve a low limit of detection (LOD), not only the detection sensitivity should be maximized but also the system noise should be minimized. Through investigation of TLS noise at different modulation frequencies, detection pinholes and flow velocities [56], it was found that in the static sample, the instrumental noise comes mainly from the shot noise of the probe beam when the chopper frequency is over 1 kHz or from the flicker noise of the probe beam at low frequencies. In the flowing sample, the flow-induced noise becomes dominant when the flow rate is high. The optimal range of the pinhole aperture to beam size ratio in the detection plane, which gave the minimum noise and thus lowest LOD, was found to be from 0.2 to 0.5 for high-modulation frequencies and from 0.05 to 0.2 for low-modulation frequencies. With the increase of the pinhole aperture to beam size ratio, the optimum on-axis pump to probe beam waist distance will decrease.

Above, we summarized the impacts of the surroundings, sample flow, beam divergence and detection pinhole aperture on the sensitivity or LOD of the system. It should be emphasized that some of the conclusions were typical for given system or sample parameters (such as modulation frequency, channel depth, beam radius and thermophysical properties of the sample and surroundings) and are only valid in that particular case. For other specific situations, new calculations or theoretical models may be required. Particularly, when the channel depth decreases to a few micrometers or even into the extended nanospace (10 nm–1 μm), the impacts of the surroundings must be considered even for the laser excitation case. Recently, Le et al. [57] proposed a new channel structure by depositing a TiO_2 layer on the bottom wall of an extended nanochannel, and thus obtained about a four-fold sensitivity enhancement for a 50 nm sample length, corresponding to a detection limit of 800 molecules in a detection volume of only 25 aL. The signal enhancement mechanism is the same as that we employed for ILS-TLM [36]. In this extended nanospace, a more detailed theoretical analysis of TL generation and detection in different channel structures should be made, which can provide a guidance to the fabrication of a specific nanochannel for the detection of a certain analyte. In addition, the beam divergence of the excitation laser can be neglected for such a thin channel but the impact of sample flow should be studied.

Contrary to conventional linear absorption-based TLMs, in which the excitation light wavelength is usually chosen in a spectral region where the analyte has maximum optical absorbance, an optical near-field (ONF) excited TLM [Fig. 2] was proposed [38], which is similar to (multiphoton) nonlinear absorption-based

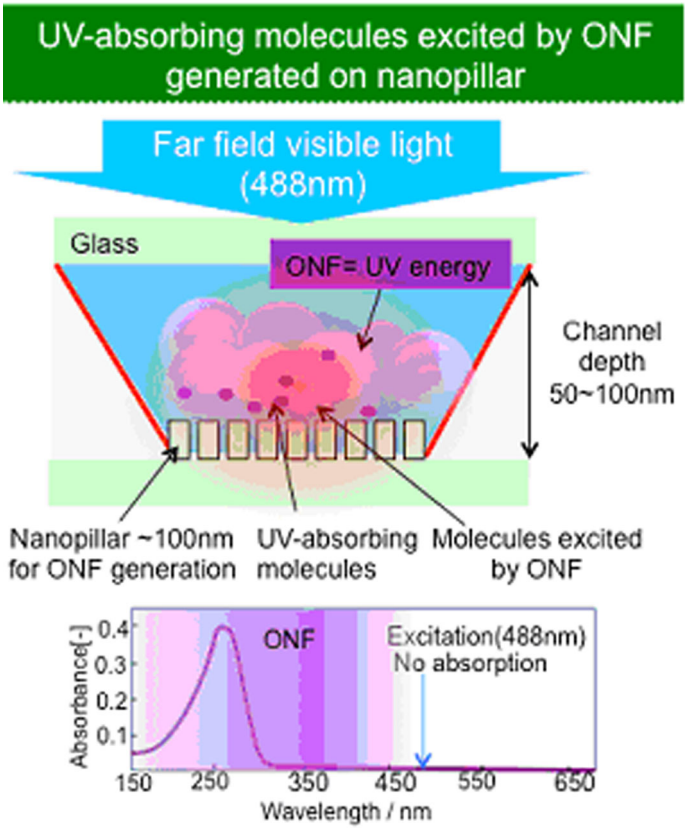

Fig. 2 Principle of an optical near-field excited TLM. Reprinted with permission from Ref. [38]. Copyright (2013) by the Chemical and Biological Microsystems Society

TLS, and employs an excitation laser whose wavelength is beyond the absorption spectral region of the analyte. Excitation of analytes is realized by the optical near-field generated on nanostructures of nonmetal materials (conceptually different from the plasmonic field enhancement on metal nanoparticles), which allows electronic excitation of molecules even though the energy of incident light is lower than the absorption energy of the molecules. Detection of UV-absorbing molecules was realized with visible excitation. This result could expand applications of visible light-based TLM in detection of biomolecules with absorption usually in UV range.

2.2 TLS for a Single Nanoparticle Detection

In recent years, TL-based photothermal microscopy was developed for the characterization of single nanoparticles (NPs). For instance, the photothermal technique is capable of detecting gold NPs with sizes down to 1.4 nm [58] or even a quencher-DNA construct (BHQ1-10T-BHQ1) with an absorption cross section of 4 angstroms^2 [49].

For small NPs, Rayleigh scattering decreases as the sixth power of diameter, and the minimum particle size to be detected in a cell or in a scattering tissue is well above 40 nm, while light absorption of a single NP decreases as only the third power of the diameter of the particle. Absorption will prevail over scattering below a certain particle size. For metal NPs, when they are excited near their plasmon resonance, they will show a relatively large absorption cross section ($\sim 6 \times 10^{-14}\text{cm}^2$ for a 5 nm diameter gold NP) and exhibit a fast electron-phonon relaxation time in the picoseconds range. The subsequent thermal relaxation of the heated NP to the surroundings will create a nanolens around the particle. In theory, interference of the nanolens on the probe beam was taken as the interference between the scattered field by the nanolens and the incident probe field.

To theoretically describe the nanolens-induced photothermal signal, on one hand, some researchers employed a direct way under certain approximations [59]: namely, the nanolens is treated as a local susceptibility fluctuation $\Delta\chi$ (Fig. 3a), and the interaction of the incident field with $\Delta\chi$ gives rise to a polarization $\boldsymbol{P}$, and then expression of the scattered field at a point M is derived by introducing the Hertz potential. In the far field where the detector is located, the scattered field varies as $1/R$ and the probe field's wavefront is assumed to be spherical, and the beat note power arriving on the detector can be expressed as the interference between the scattered and probe fields. Recently, a more rigorous theoretical model based on GLMT was used for describing the photothermal signal of a single NP [34]. In this model, the heated NP-generated photothermal nanolens was regarded as a superposition of N layers, each of which has its own refractive index, as shown in Fig. 3b. By applying GLMT to this discretized nanolens, the near or far field light intensity distributions can be calculated, and correspondingly, the photothermal signal can be achieved. Through analysis, Selmeke et al. found that the following: (1) the photothermal signal varies approximately linear with the axial particle position z_p within a range of 200 nm around the inflection point. This yields some perspectives for measuring small amplitude motions or even small particle displacements, such as in biological samples. (2) The sharp separation of the two lobes extended the photothermal correlation spectroscopy techniques [50], in which both the autocorrelation of the signal magnitude and the cross-correlations of positive and negative signals become accessible and allow for the detection of anisotropic and directed motion. (3) The measured signal strongly depends on the shape of the refractive index profile even if the absorption cross section of the object is the same. A calibration will hence only give reasonable results when a comparative signal comes from the same type of spatial refractive index shape (i.e. inverse distance dependencies). With some exciting achievements, the analysis is, however, incomplete since it is based on a simple case (a steady-state temperature profile and a nonlocalized surrounding environment). Therefore, a more detailed investigation of the photothermal signal behaviour under different experimental conditions (including the NP size/material, surrounding environment size/material, laser parameters (modulation frequency, cw or pulsed excitation) and relative position of the NP to the pump/probe beams) is desirable, which would provide great value for specific applications or even pave the way for new developments.

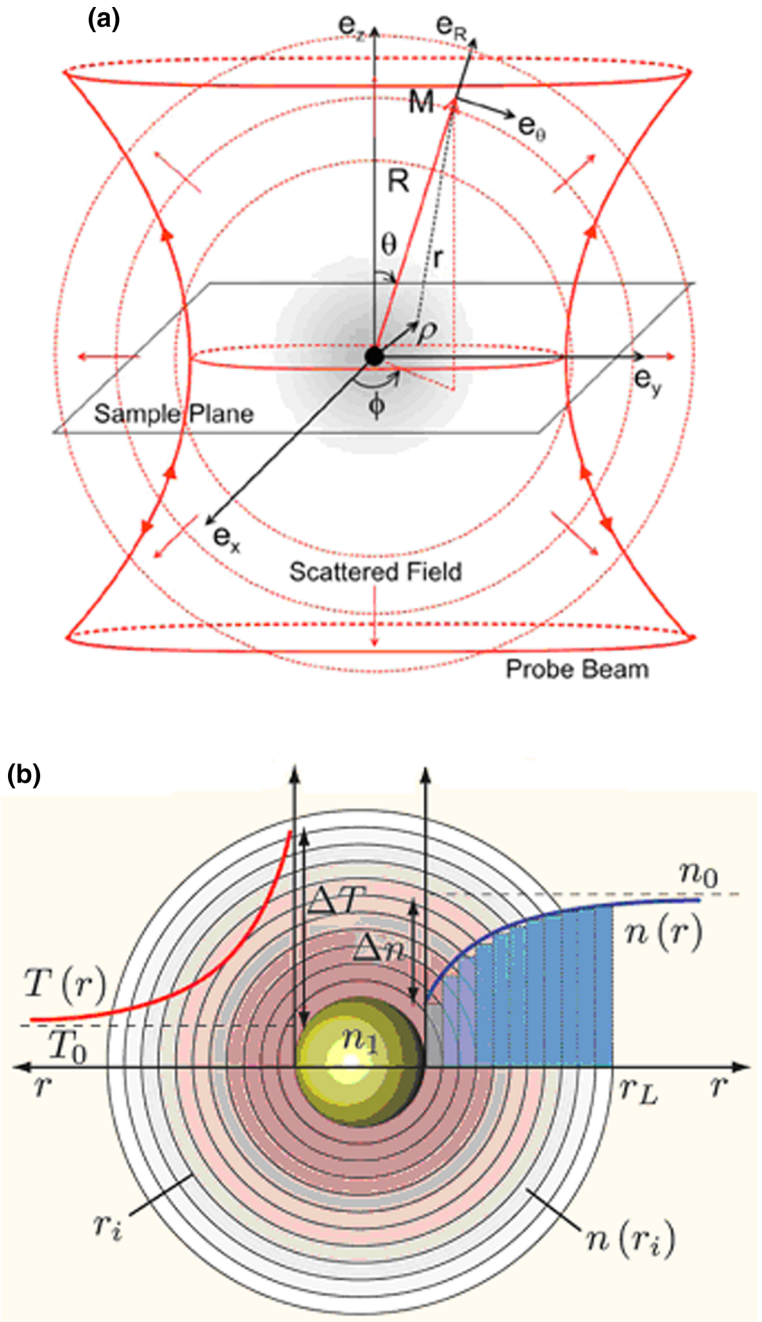

Fig. 3 (a) Schematic representation of the interaction of the probe beam and a nanolens (treated as a local susceptibility). Reprinted with permission from Ref. [59]. Copyright (2006) by the American Physical Society. (b) Illustration of the temperature profile $T(r)$, the refractive index profile $n(r)$, and the discretization of the latter. Reprinted with permission from Ref. [34]. Copyright (2012) by the American Chemical Society

3 Applications of TLS and TLM

3.1 Chemical, Biomedical and Environmental Analysis

Although TLM has many advantages over TLS in terms of spatial and temporal resolutions, portability and applicability to microscale analytical devices, TLS is still commonly used for detection of analytes when the detection sensitivity or time-resolved TLS signal is of concern.

TLS was applied for the characterization of new (heterogeneous) materials, such as fullerenes and nanodiamond dispersions, which are promising materials in the production of composites and catalysts for biomedicine and biotechnology. However, their applications remain limited because their dispersions are not fully characterized and consequently difficult to regulate. To obtain information regarding the concentration of fullerenes and nanodiamonds in solutions and the size of individual colloidal particles, aggregates and clusters, Proskurnin et al. [26–28] recently employed TLS for characterization of their optical and colloidal properties. They showed the distinction between aqueous fullerene dispersions (AFDs) in comparison with organic solutions of fullerenes caused by the formation of large clusters, and measured the kinetics of coagulation of AFDs using strong acids and increasing ionic strength at various concentration levels. Thermophysical parameters (thermal diffusivity, thermal conductivity, and thermal effusivity) of AFDs were measured by the time-resolved curves. The LODs for C60 and C70 fullerenes are approximately $100 \text{ng} \cdot \text{mL}^{-1}$, which are 20-fold lower when compared to conventional spectrophotometry. Estimation of the size of AFDs by TLS is in good concordance with dynamic light scattering and small-angle neutron scattering data. Unfortunately, the theory, which binds the size and the nature of the disperse particles and the behaviour of the transient curve is still not fully developed, and only an estimation of the range of the particle/aggregate/cluster size can be made. Further work should be focused on the improvement of the theoretical models and their use for characterizing the dispersions.

In order to improve the selectivity, TLS is often combined with separation techniques, such as chromatographic techniques, electrophoretic techniques and bioanalytical techniques (immunoassay or enzymatic reaction-based analysis). Recently, direct analysis of free bilirubin in human and animal blood serum samples was realized by HPLC-TLS [30]. This hyphenated method enabled a baseline separation of all three structural isomers of bilirubin (XIII-α, IX-α and III-α) and the respective degradation products in isocratic mode in less than seven minutes. The method excels in ultra-high sensitivity with LOD and limit of quantitation (LOQ) of 90 pM and 250 pM, respectively, 20 times lower than those obtained with HPLC-DAD. The high sensitivity enabled to simplify streamline sample preparation to just one serum ultrafiltration step, which made qualitative evaluation of sample preparation possible for the first time. Furthermore, free bilirubin was for the first time detected in human vascular endothelial cells and its intracellular antioxidant activity was demonstrated in nM range [60].

In microspace, a combined microfluidic flow injection analysis-TLM (μFIA-TLM) was applied for the determination of neutrophil gelatinase-associated lipocalin (NGAL)—a biomarker of acute kidney injury [44]. At an excitation power of 100mW,

the μFIA-TLM provided about seven times lower LOD ($1.5 pg \cdot mL^{-1}$) in comparison to a conventional ELISA test, and a sample throughput of six samples per minute, which compares favourably with sample throughput of the microtiter plate reader. Comparison of NGAL dynamics in patients undergoing coronary angiography measured with transmission mode spectrometry on a microtiter plate reader and with μFIA-TLM showed good agreement. Quite recently, ELISA of NGAL was transferred into a microfluidic chip [61], where NGAL antibodies were immobilized onto magnetic nanobeads retained in the microchannel by magnets. In-chip ELISA was successfully realized for NGAL analysis with a detection limit of 5 pg/mL and a total analysis time of 35 min, which is much shorter than that of four hours in a microtiter plate well-based ELISA.

For the applications in environmental and food safety analysis, which were reviewed recently [62], the μFIA-TLM system was applied for rapid and sensitive detection of Cr(VI) [62,63] based on colorimetric reaction with diphenylcarbazide which yields chromium-diphenylcarbazone (Cr-DPCO) complexes absorbing at 540 nm. Compared to the conventional FIA-TLS [64], detection of Cr(VI) in μFIA-TLM reduces the sample/reagent consumption over 100 times to submicroliter volumes and the time for one sample injection over 10 times to only a few seconds. However, like most metal-DPCO complexes, Cr-DPCO is also photolabile [13,65], and when the average number of absorbed photons per each Cr-DPCO complex was above the threshold of around 1600, photodegradation of the Cr-DPCO complex could be clearly observed also in μFIA-TLM. For high-power excitations, increasing the flow rate can alleviate photodegradation of the complex to some extent (about 8 % when increasing the flow rate from 20 to 50 μL/min). Concurrently, this decreased the diffusion broadening of the μFIA-TLM peaks and enabled up to 20 injections of sample per minute, which is a substantial improvement compared to over 30 seconds needed for one injection in FIA-TLS [64]. The LOD for Cr(VI) in a 50 μm deep microchannel was estimated at ng/mL concentration level.

In addition, based on the previous FIA-TLS results [62], protein phosphatase inhibition assay (PPIA) of microcystin-LR—the most toxic microcystin in the family of cyanotoxin—was developed in a μFIA-TLM system [43]. For the protein phosphatase-substrate reaction, the product generation rate in a microfluidic chip was over eight times faster than in an eppendorf tube, corresponding to reduction of the analysis time from about 30 min in a microtiter plate well to a few min in a microchip. The LOD is 80 ng/L (over 10 times lower than the maximal contaminant level set for microcystin by WHO), which is over three times lower than that obtained by a microtiter plate PPIA kit (Abraxis) or 1.3 times lower than that by a commercial ELISA kit (Enzo). The linearity range for the μFIA-TLM PPIA is 0.08-1 μg/L.

In practical applications of TLM in lab-on-a-chip devices, one critical problem, which would disable a repeatable and accurate measurement over a long period of time, is the contamination of the microchannel wall, especially when a high-power laser is used for heating the sample. This problem is power density (especially near the channel wall) and sample dependent. For regular measurement in a microchannel, where different analytes could be the detection target, the pump laser should be focused to the diffraction limit and this diffraction-limited spot should be positioned in the middle of the channel in order to minimize contamination to the channel wall,

even though there is an optimum pump beam waist radius from the point of view of sensitivity enhancement for relatively thick microchannels as we discussed above [35]. For ultra-thin channels (a few micrometers or submicrometer), in order to alleviate this problem, we should use lower laser power, avoid use of sticky compounds or those compounds liable to accumulate on the wall under laser heating, and if possible, perform the detection in flowing mode. Once pollution occurs, the measurement should be suspended and a cleaning procedure should be performed by flushing the channel with solvents such as acetone, relatively strong acids or bases.

3.2 Single Nanoparticle-Based Photothermal Microscopy, Imaging and Subnanosecond Time-Resolved Microscopy

The nanoparticle-based photothermal microscopy (PTM) can not only be used for characterizing the properties (absorption, dynamic behaviour) of the nanoparticle itself in different environments, but also be widely applied for imaging of (biological) structures when they are labelled with metal nanoparticles or organic molecules (melanin, heme proteins and chlorophyll) [54].

One of the applications of the PTM is to perform absorption spectroscopy of individual nanostructures, such as studying plasmon resonance and its intrinsic broadening of individual metallic nanoparticles [66], extracting biexciton and trion binding energies of individual semiconductor nanocrystals [67], or determining the absorption of single-wall carbon nanotubes [68], although the results would not highly accurate, since the photothermal signal is dependent on the parameters of both the NP and the surroundings (as stated in Sect. 2.2). For investigation of dynamic processes of molecules/NPs, photothermal correlation spectroscopy was used for quantitative determination of the diffusion constant of nanoparticles and measurement of the hydrodynamic diameter of functionalized nanoparticles [69,70].

Photothermal microscopy can be used for imaging or single particle tracking in micro-environments. A 5 nm gold nanoparticle functionalized with a green fluorescence protein (GFP) nanobody (with a final size of less than 10 nm), was used to label surface and intracellular GFP-proteins in environments such as adhesion sites and cytoskeletal structures [71], which allows long-time observation of small nanometer-sized labels. To achieve fast imaging of moving objects, which cannot be resolved during a raster scan, Lasne et al. designed a triangulation-based tracking scheme in order to record the trajectories of single membrane proteins in live cells at a video rate [72], allowing to record the full history of proteins in cells including intermediate states due to the high photothermal signal stability.

For fast wide-field imaging using a CCD camera, PTM with optical lock-in detection was used. Pache et al. developed a photothermal lock-in optical coherence microscopy (poli-OCM) for the detection of single 40 nm gold particles with a 0.5μm lateral and 2μm axial resolutions over a 50 μm depth of field [73]. Both the intensity of the heating beam and the phase of the reference beam were modulated by acousto-optic modulators, and the interference between the reference and the back-scattered fields gives a poli-OCM signal I_{poli} (interference between E_r and E_{poli}) and a dark-field OCM signal I_{df} (interference between E_r and E_{df}). By setting the integration time of

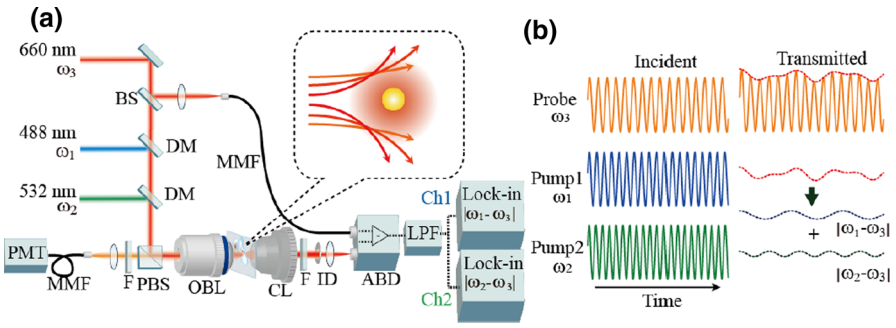

Fig. 4 (a) Schematic representation of the experimental setup of a dual-wavelength photothermal microscope using intensity-modulated lasers and (b) its principle: the pump beam intensities are modulated at ω_1 and ω_2, and the probe beam intensity is modulated at ω_3. Beat signals are generated by the photothermal effect at the sample position. Reprinted with permission from Ref. [82]. Copyright (2015) by the Optical Society of America

the line camera to an integer multiple m of periods of the modulation frequency, the integrated background was eliminated and the tomogram S(z) was derived from the Fourier transform of the integrated poli-OCM signal $\langle I_{poli} \rangle$. Compared with previous photothermal optical coherence tomography (OCT) setups, which required the acquisition of multiple axial profiles at the same lateral position [74,75], this scheme maintained the speed advantage of OCT. However, in a lateral direction, this method still employed a raster-scanning mode. In order to realize fast wide-field imaging in lateral direction, Eldridge developed a photothermal setup allowing for co-registered quantitative phase imaging (QPI) in an off-axis holography scheme [76]. An S/N ratio of 103 was obtained for NP-tagging of an epidermal growth factor receptor (EGFR) in live cells with a three second acquisition.

The laser sources used in PTM are mostly CW lasers, while in the time-resolved [77] and nonlinear PTM [78] nanosecond solid-state lasers were used as the source of the pump beam. Kobayashi et al. presented a scheme for time-resolved pump-probe microscopy based on intensity-modulated laser diodes or picosecond pulses spectrally filtered from a compact supercontinuum fibre laser source [79–82]. By modulating the pump and probe beams (up to 500 MHz with fixed frequency detuning typically at ∼10 kHz) (Fig. 4), frequency response of the beat-frequency signal is recorded, which can be used for characterizing nanosecond to picosecond photo-excitation processes of sample species (such as dynamics of photoexcited carriers, reaction intermediates and triplet state molecules) without the need of a high-speed detector or a high-frequency lock-in amplifier. However, it is difficult to resolve sub-picosecond dynamics, which can be readily measured using mode-locked pulse lasers. Moreover, the time-resolved pump-probe photothermal microscopy provides better spatial resolution than the conventional diffraction-limited optical microscopes since the pump-probe signal is based on the nonlinear interaction between the two laser beams and the sample. The reported spatial resolution of such nonlinear photothermal microscopy is ∼188 nm. This is ∼23 % better than for commonly utilized linear photothermal microscopy as achieved experimentally and ∼43 % better than theoretically predicted for conventional optical microscopy. In addition, the imaging system is much less affected by thermal blurring than photothermal microscopes with CW light sources.

4 Conclusions

There are a few drawbacks in the present TLS/TLM, which open opportunities for further progress: (1) the instruments are not user-friendly, because professionals are needed especially when the system is misaligned or the system configuration needs to be changed for some specific analysis; (2) the instruments lack tunability/versatility since they are usually working at one or a few laser lines only; (3) in extended nanospace, more theoretical and experimental research is required in order to enable sensitive detection in such ultra-small space. Correspondingly, in the future, we should focus on following research activities: (1) development of automated TLS/TLM instruments, in which beam alignment and system optimization could be made automatically; (2) development of broadband TLS/TLM, in which an incoherent light source or supercontinuum light source can be incorporated; (3) development of theoretical models for TLM or photothermal microscopy in complex ultra-small (extended nano) space, and undertake a detailed investigation of photothermal signals under different systematic parameters in order to find some solutions for sensitivity enhancement in such a small space, or to a further step, development of new TLMs based on new physical effects in nanospace (such as optical near fields).

Along with the development of TLS/TLM instruments, more applications of the photothermal lens technique in different fields should be explored. For example, the performance-enhanced photothermal microscopy can be used for high-throughput sample detection in microfluidic chip (micro-HPLC or micro-ELISA), for thermophysical property characterization of new materials (mesoporous materials, soft matters, super thin, nanostructured and precious metal-doped nanocomposite semiconductors), or for monitoring physical, chemical or biological processes, such as local phase transitions (which occur on length scales of a few nanometres and typically involve strong refractive index changes). By combining with nanothermometer (such as nitrogen vacancy-based nanoscale thermometer [83]), photothermal lens microscopy can be used for localized heating or to regulate temperature change in biological cells, which is important for studying the impact of temperature on the biological activities in cells or other temperature-sensitive phenomena.

References

1. S.E. Bialkowski, *Photothermal Spectroscopy Methods for Chemical Analysis* (Whiley, New York, 1996)
2. M. Franko, Appl. Spectrosc. Rev. **43**, 358 (2008)
3. D. Comeau, A. Haché, Appl. Phys. Lett. **83**, 246 (2003)
4. M.E. Long, R.L. Swofford, A.C. Albrecht, Science **191**, 183 (1976)
5. M. Liu, Combined TLS and microfluidic-FIA devices for highly sensitive and rapid environmental analysis, PhD thesis, University of Nova Gorica, Nova Gorica, 2013, pp.7–17
6. J.D. Ingle, S.R. Crouch Jr., *Spectrochemical Analysis* (Prentice Hall, New Jersey, 1988)
7. M. Franko, C.D. Tran, Rev. Sci. Instrum. **67**, 1 (1996)
8. M. Franko, in *Encyclopedia of Analytical Chemistry*, ed. by R.A. Meyers, C.D. Tran (Wiley, Chichester, 2011), pp. 1249–1279
9. T. Kitamori, M. Tokeshi, A. Hibara, K. Sato, Anal. Chem. **76**, 52A (2004)
10. H. Cabrera, E. Sira, K. Rahn, M. García-Sucre, Appl. Phys. Lett. **94**, 051103 (2009)

11. H. Cabrera, F. Cordido, A. Velásquez, P. Morenoa, E. Sira, S.A. López-Rivera, C. R. Mec. **341**, 372 (2013)
12. P. Kumar, A. Khan, D. Goswami, Chem. Phys. **441**, 5 (2014)
13. P.R.B. Pedreira, L.R. Hirsch, J.R.D. Pereira, A.N. Medina, A.C. Bento, M.L. Baesso, M.C. Rollemberg, M. Franko, J. Shen, J. Appl. Phys. **100**, 044906 (2006)
14. N.G.C. Astrath, F.B.G. Astrath, J. Shen, J. Zhou, K.H. Michaelian, C. Fairbridge, L.C. Malacarne, P.R.B. Pedreira, P.A. Santoro, M.L. Baesso, Appl. Phys. Lett. **95**, 191902 (2009)
15. A.V. Brusnichkin, D.A. Nedosekin, M.A. Proskurnin, V.P. Zharov, Appl. Spectrosc. **61**, 1191 (2007)
16. A. Marcano, H. Cabrera, M. Guerra, R.A. Cruz, C. Jacinto, T. Catunda, J. Opt. Soc. Am. B **23**, 1408 (2006)
17. R. Antonio Cruz, A. Marcano, C. Jacinto, T. Catunda, Opt. Lett. **34**, 1882 (2009)
18. C. Jacinto, T. Catunda, D. Jaque, J. García Solé, A.A. Kaminskii, J. Appl. Phys. **101**, 023113 (2007)
19. A.A. Andrade, S.A. Lourenço, V. Pilla, A.C.A. Silva, NoelioO Dantas, Phys. Chem. Chem. Phys. **16**, 1583 (2014)
20. A.N.G. Parra-Vasquez, L. Oudjedi, L. Cognet, B. Lounis, J. Phys. Chem. Lett. **3**, 1400 (2012)
21. W.-S. Chang, S. Link, J. Phys. Chem. Lett. **3**, 1393 (2012)
22. M. Ventura, E. Simionatto, L.H.C. Andrade, E.L. Simionatto, D. Riva, S.M. Lima, Fuel **103**, 506 (2013)
23. W.C. Silva, A.M. Rocha, M. Priscila, P. Castro, M.S. Sthel, H. Vargas, G.F. David, V.H. Perez, Fuel **130**, 105 (2014)
24. J.F. Sánchez Ramírez, J.L. Jiménez Pérez, R. Carbajal Valdez, A. Cruz Orea, R. Gutiérrez Fuentes, J.L. Herrera-Pérez, Int. J. Thermophys **27**, 1181 (2006)
25. A. Marcano O, F. Delima, Y. Markushin, N. Melikechi, J. Opt. Soc. Am. B **28**, 281 (2011)
26. I.V. Mikheev, D.S. Volkov, M.A. Proskurnin, M.V. Korobov, Int. J. Thermophys. **36**, 956 (2015)
27. I. V. Mikheev, D. S. Volkov, M. A. Proskurnin, M. V. Korobov, Monitoring of Aqueous Fullerene and Nanodiamond Dispersions Using Photothermal and Photoacoustic Spectroscopy. in X*II International Conference on Nanostructured Materials (NANO 2014)*, Moscow, 13–18 July 2014
28. D.S. Volkov, M.A. Proskurnin, I.V. Mikheev, D.V. Vasil'ev, M.V. Korobov, D.A. Nedosekin, V.P. Zharov, Application of Photothermal and Photoacoustic Spectroscopy for the Monitoring of Aqueous Dispersions of Carbon Nanomaterials, Advanced Laser Technologies (ALT) 12, 2–6 Sept, 2012, Thun. doi:10.12684/alt.1.94
29. D.A. Nedosekin, N.V. Saranchina, A.V. Sukhanov, N.A. Gavrilenko, I.V. Mikheev, M.A. Proskurnin, Appl. Spectrosc. **67**, 709 (2013)
30. M. Martelanc, L. Žiberna, S. Passamonti, M. Franko, Anal. Chim. Acta **809**, 174 (2014)
31. A.V. Brusnichkin, D.A. Nedosekin, E.I. Galanzha, Y.A. Vladimirov, E.F. Shevtsova, M.A. Proskurnin, V.P. Zharov, J. Biophoton. **3**, 791 (2010)
32. M. Liu, D. Korte, M. Franko, J. Appl. Phys. **111**, 033109 (2012)
33. J. Moreau, V. Loriette, Jpn. J. Appl. Phys. **45**, 7141 (2006)
34. M. Selmke, M. Braun, F. Cichos, ACS Nano **6**, 2741 (2012)
35. M. Liu, M. Franko, Appl. Phys. B **115**, 269 (2014)
36. M. Liu, M. Franko, Appl. Phys. Lett. **100**, 121110 (2012)
37. K. Mawatari, T. Ohashi, T. Ebata, M. Tokeshic, T. Kitamori, Lab Chip **11**, 2990 (2011)
38. T. H. H. Le, K. Mawatari, H. Shimizu, T. Yatsui, T. Kawazoe, M. Naruse, M. Ohtsu, and T. Kitamori, Novel detection of non-absorbing molecules by optical near-field induced thermal lens microscopy. in *17th International Conference on Miniaturized Systems for Chemistry and Life Sciences*, 27–31 Oct 2013, Freiburg, pp. 675–677
39. K. Mawatari, S. Kubota, T. Kitamori, Anal. Bioanal. Chem. **391**, 2521 (2008)
40. J. Zhang, Y. Huang, C.-J. Chuang, M. Bivolarska, C.W. See, M.G. Somekh, M.C. Pitter, Opt. Express **19**, 2643 (2011)
41. H. Shimizu, K. Mawatari, T. Kitamori, Anal. Chem. **82**, 7479 (2010)
42. H. Katae, S. Hirashima, A. Harata, J. Phys. **214**, 012122 (2010)
43. M. Liu, I. Fonda, and M. Franko, Rapid and Sensitive Detection of Microcystin by Microfluidic Flow Injection Thermal Lens Microscopy. in *18th International Conference on Photoacoustic and Photothermal Phenomena*, Novi Sa, 6–10 Sept 2015
44. T. Radovanović, M. Liu, P. Likar, M. Klemenc, M. Franko, Int. J. Thermophys. **36**, 932 (2015)
45. D.A. Nedosekin, E.I. Galanzha, S. Ayyadevara, R.J.S. Reis, V.P. Zharov, Biophys. J. **102**, 672 (2012)
46. D.A. Nedosekin, E.I. Galanzha, E. Dervishi, A.S. Biris, V.P. Zharov, Small **10**, 135 (2014)
47. M. Lubej, U. Novak, M. Liu, M. Martelanc, M. Franko, I. Plazl, Lab Chip **15**, 2233 (2015)

48. H. Shimizu, K. Mawatari, T. Kitamori, Analyst **139**, 2154 (2014)
49. A. Gaiduk, M. Yorulmaz, P.V. Ruijgrok, M. Orrit, Science **330**, 353 (2010)
50. M. Selmke, R. Schachoff, M. Braun, F. Cichos, RSC Adv. **3**, 394 (2013)
51. C.L. Cassano, K. Mawatari, T. Kitamori, Z.H. Fan, Electrophoresis **35**, 2279 (2014)
52. M. Liu, M. Franko, Crit. Rev. Anal. Chem. **44**, 328 (2014)
53. A. Gaiduk, P.V. Ruijgrok, M. Yorulmaz, M. Orrit, Chem. Sci. **1**, 343 (2010)
54. P. Vermeulen, L. Cognet, B. Lounis, J. Microsc. **254**, 115 (2014)
55. M. Liu, U. Novak, I. Plazl, M. Franko, Int. J. Thermophys. **35**, 2011 (2014)
56. M. Liu, M. Franko, Int. J. Thermophys. **35**, 2178 (2014)
57. T.H.H. Le, K. Mawatari, H. Shimizu, T. Kitamori, Analyst **139**, 2725 (2014)
58. S. Berciaud, L. Cognet, G.A. Blab, B. Lounis, Phys. Rev. Lett. **93**, 257402 (2004)
59. S. Berciaud, D. Lasne, G.A. Blab, L. Cognet, B. Lounis, Phys. Rev. B **73**, 045424 (2006)
60. L. Žiberna, M. Martelanc, M. Franko, S. Passamonti, Presence and Modulation of Endogenous Bilirubin In the Human Vascular Endothelial Cells (in preparation)
61. T. Radovanović, U. Novak, S. Kralj, M. Liu, P. Žnidaršič Plazl, M. Franko, Thermal lens microscopy in a new magnetic nanobeads based ELISA assay on microchip for detection of contrast-induced acute kidney injury. in *18th International Conference on Photoacoustic and Photothermal Phenomena*, Novi Sad, 6–10 Sept 2015
62. M. Franko, M. Liu, A. Boškin, A. Delneri, M.A. Proskurnin, Anal. Sci. **32**, 23 (2016)
63. T. Gor'kova, M. Liu, M. Proskurnin, M. Franko, Determination of trace Cr(VI) with diphenylcarbazide by μFIA-thermal lens microscopy. Acta Chim. Slov. (2016) (Submitted to)
64. A. Madžgalj, M.L. Baesso, M. Franko, Eur. Phys. J. Spec. Top. **153**, 503 (2008)
65. P.R.B. Pedreira, L.R. Hirsch, J.R.D. Pereira, A.N. Medina, A.C. Bento, M.L. Baesso, M.C.E. Rollemberg, M. Franko, Chem. Phys. Lett. **396**, 221 (2004)
66. S. Berciaud, L. Cognet, P. Tamarat, B. Lounis, Nano Lett. **5**, 515 (2005)
67. S. Berciaud, L. Cognet, B. Lounis, Nano Lett. **5**, 2160 (2005)
68. S. Berciaud, L. Cognet, B. Lounis, Phys. Rev. Lett. **101**, 077402 (2008)
69. V. Octeau, L. Cognet, L. Duchesne, D. Lasne, N. Schaeffer, D.G. Fernig, B. Lounis, ACS Nano **3**, 345 (2009)
70. C. Leduc, J. Jung, R.R. Carney, F. Stellacci, B. Lounis, ACS Nano **5**, 2587 (2011)
71. C. Leduc, S. Si, J. Gautier, M. Soto-Ribeiro, B. Wehrle-Haller, A. Gautreau, G. Giannone, L. Cognet, B. Lounis, Nano Lett. **13**, 1489 (2013)
72. D. Lasne, G.A. Blab, S. Berciaud, M. Heine, L. Groc, D. Choquet, L. Cognet, B. Lounis, Biophys. J. **91**, 4598 (2006)
73. C. Pache, N.L. Bocchio, A. Bouwens, M. Villiger, C. Berclaz, J. Goulley, M.I. Gibson, C. Santschi, T. Lasser, Opt. Express **20**, 21385 (2012)
74. M.C. Skala, M.J. Crow, A. Wax, J.A. Izatt, Nano Lett. **8**, 3461 (2008)
75. Y. Jung, R. Reif, Y. Zeng, R.K. Wang, Nano Lett. **11**, 2938 (2011)
76. W.J. Eldridge, A. Meiri, A. Sheinfeld, M.T. Rinehart, A. Wax, Biomed. Opt. Express **5**, 2517 (2014)
77. D. Lapotko, T. Romanovskaya, A. Shnip, V. Zharov, Lasers Surg. Med. **31**, 53 (2002)
78. D. Nedosekin, E. Galanzha, E. Dervishi, A. Biris, V. Zharov, Small **10**, 135 (2014)
79. J. Miyazaki, K. Kawasumi, T. Kobayashi, Rev. Sci. Instrum. **85**, 093703 (2014)
80. J. Miyazaki, H. Tsurui, A. Hayashi-Takagi, H. Kasai, T. Kobayashi, Opt. Express **22**, 9024 (2014)
81. J. He, J. Miyazaki, N. Wang, H. Tsurui, T. Kobayashi, Opt. Express **23**, 9762 (2015)
82. J. Miyazaki, H. Tsurui, K. Kawasumi, T. Kobayashi, Opt. Express **23**, 3647 (2015)
83. G. Kucsko, P.C. Maurer, N.Y. Yao, M. Kubo, H.J. Noh, P.K. Lo, H. Park, M.D. Lukin, Nature **500**, 54 (2013)